Available online at www.sciencedirect.com

ScienceDirect

Procedia Structural Integrity 54 (2024) 107–114

Structural Integrity Procedia

www.elsevier.com/locate/procedia

International Conference on Structural Integrity 2023 (ICSI 2023)

On the use of full-field receptances in inverse vibro-acoustics for airborne structural dynamics

Alessandro Zanarini*

DIN, Industrial Engineering Dept., University of Bologna, Viale Risorgimento 2, 40136 Bologna, Italy

Abstract

Dynamic airborne pressure fields may become a concern for the excitation of lightweight structures and components in aerospace and automotive engineering. Full-field optical techniques can nowadays estimate accurate receptance maps to describe the frequency domain relation between excitation forces and displacement maps on lightweight components, where the inertia-related distortions of traditional transducers are not allowed. The usage of the receptances in the Rayleigh integral approximation of sound radiation from a vibrating surface is here followed in early attempts of inverse vibro-acoustics, with the aim to identify, once the airborne pressure field is known in its spectrum, the broad frequency band force that is transmitted to the excitation points used in the direct FRF problem. Details and considerations on the inverse formulation of the problem, together with examples coming from a real thin plate tested, are provided in this work.

Keywords: full-field dynamic testing; full-field FRFs; Rayleigh integral approximation; inverse vibro-acoustics; airborne loading; force identification.

1. Introduction

The distributed dynamic loading, coming from airborne pressure fields, may excite excessively the modal base or may shorten the life of the actual realisation. Many times the sound radiation simulations from structural vibrations in NVH studies are run with linear structural FE models, potentially simplified on the treatment of boundary conditions, frictions, damping, mistuning from actually produced parts and non-linearities. Instead, working with full-field optical *receptances*, coming from broad frequency band real testing (see Van der Auweraer et al. (2001); Zanarini (2005b,a, 2007, 2014a,b, 2015b,a,d, 2018, 2019a,b, 2020, 2022b) for enhanced structural dynamics assessments and model updating; see instead Zanarini (2008a,b, 2015c, 2022f,e,c,a, 2023c) for enhancements of fatigue spectral methods and failure risk grading), may represent a viable path in order to have the best achievable representation of the real behaviour of manufactured and mounted components around their working load levels, also with modally dense structural dynamics and complex patterns in the dynamic signature of the excitations.

* Corresponding author. Tel +39 051 209 3442.
E-mail address: a.zanarini@unibo.it (Alessandro Zanarini).

10.1016/j.prostr.2024.01.062

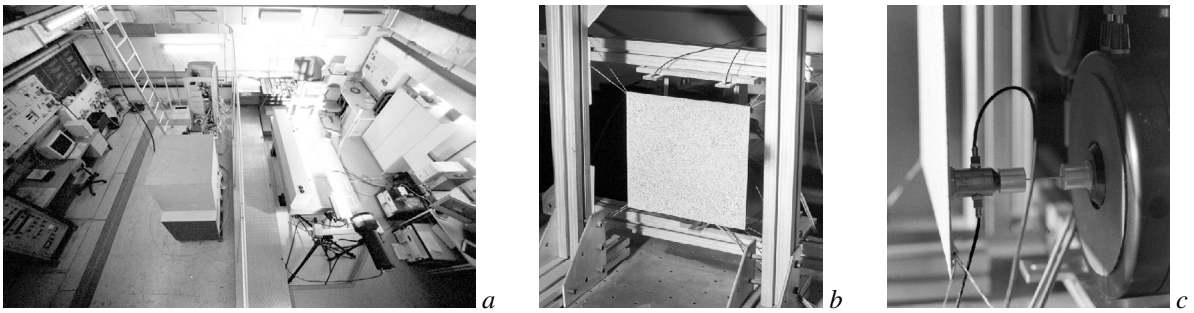

Fig. 1. The lab in the TEFFMA project (see Zanarini (2014a,b, 2015b,a,c,d, 2018, 2019a,b, 2022b)): aerial view in *a*, restrained plate sample in *b*, 2 shakers on the back of the plate in *c*.

The *experiment-based optical full-field receptances* proved to work (see Zanarini (2022d, 2023a,b)) also in the Rayleigh integral approximation of the sound propagated in the free-field acoustic domain by the characterised surface, for the numerical approximation of the spectral relation among the sound radiation field, the structural dynamics and excitation forces. The same background (see also Wind et al. (2006)), reformulated in Section 2 with notes for the inverse vibro-acoustics, is here followed in early attempts of inverse airborne vibro-acoustics by means of the *full-field experiment-based receptances* obtained in the TEFFMA project, with the aim to identify, once the airborne pressure field is known in its spectrum, the broad frequency band force that is transmitted to the excitation points used in the direct FRF problem. This identification may permit the airborne structural dynamics' characterisation of the components under test for further dynamic displacement and strain/stress distribution studies.

A recall of the experiment-based FRF modelling is sketched in Section 3, with a brief description of the testing set-up of Fig.1. The specimen under test was the simple thin rectangular plate of the TEFFMA project, designed as a lightweight structure to retain a complex structural dynamics within the operative ranges of the used measurement technologies, with its real constraints and damping characteristics.

In Section 4 examples are given in the space and frequency domains, after notes on the meshing of the acoustic domain, with special attention on the multi-modal superposition, also outside the eigenfrequencies, and on the contribution of the *experiment-based full-field receptance maps* to the accuracy of the radiated acoustic pressure FRFs & fields, and their inversions to identify the force on a structural location induced by the modelled airborne pressure fields, before drawing the reader's attention to Section 5 for the final conclusions.

2. Sound pressure & inverse vibro-acoustic formulation

In the case of propagating waves as in Mas and Sas (2004), according to Kirkup (1994); Desmet (2004); Wind et al. (2006); Kirkup and Thompson (2007); Kirkup (2019), in the $a-th$ point of global coordinates $\boldsymbol{a}_a$ of the acoustic domain A, or air, the sound pressure $p(\boldsymbol{a}_a,\omega)$ can be defined from the Helmholtz equation as:

$$p(\boldsymbol{a}_a,\omega) = 2i\omega\rho_0 \int_S v_n(\boldsymbol{q}_q,\omega)G(r_{aq},\omega)dS, G(r_{aq},\omega) = \frac{e^{-ikr_{aq}}}{4\pi r_{aq}} = \frac{e^{-i\omega r_{aq}/c_0}}{4\pi r_{aq}}, \tag{1}$$

where i is the imaginary unit, ω is the angular frequency ($\omega = 2\pi h$, with h being the time frequency in Hertz), ρ_0 is the medium (air) density, $v_n(\boldsymbol{q}_q,\omega)$ is the normal (out-of-plane) velocity of the infinitesimal vibrating surface dS located in the global coordinate $\boldsymbol{q}_q$, $\boldsymbol{q}$ representing the whole vector of coordinates of the vibrating surface S, $k = \omega/c_0 = 2\pi/\lambda$ is the wavenumber in the Helmholtz equation (c_0 is the speed of sound at rest in the medium, λ is the acoustic wavelength), $r_{aq} = \|\boldsymbol{r}_{aq}\|$ is the norm of the distance $\boldsymbol{r}_{aq} = \boldsymbol{a}_a - \boldsymbol{q}_q$ between the points in the two domains, and $G(r_{aq},\omega)$ is the free space Green's function as described in Eq.1.

The normal velocities in the frequency domain are linked to the dynamic out-of-plane displacements over the static configuration $\boldsymbol{q}$, by means of the relation $\boldsymbol{v}_n(\boldsymbol{q},\omega) = -i\omega\boldsymbol{d}_n(\boldsymbol{q},\omega)$, which are expressions, by $\boldsymbol{d}_n(\boldsymbol{q},\omega) = \boldsymbol{H}_{d_n q f}(\omega)\cdot$

$\boldsymbol{F}_f(\omega)$, of the *receptance FRFs* $\boldsymbol{H}_{\boldsymbol{d}_n\boldsymbol{q}f}(\omega)$ of size $N_q \times N_f$ - being N_q the number of the outputs and N_f of the inputs - and of the *excitation signatures* $\boldsymbol{F}_f(\omega)$. Eq.1 can be therefore rewritten in terms of a sum of discrete contributions, by means of a discretisation of the vibrating surface domain $S \approx \sum_q \Delta S_q$ that scatters the sound pressure:

$$p(\boldsymbol{a}_a, \omega) \approx -2\omega^2\rho_0 \sum_q^{N_q} \boldsymbol{H}_{\boldsymbol{d}_n q f}(\omega)\boldsymbol{F}_f(\omega)G_{aq}(r_{aq}, \omega)\Delta S_q \in \mathbb{C}, \tag{2}$$

with $\boldsymbol{H}_{\boldsymbol{d}_n\boldsymbol{q}f}(\omega)$, $\boldsymbol{F}_f(\omega)$ and $G_{aq}(r_{aq}, \omega)$ as *complex-valued* discrete quantities, $r_{aq} = \|\boldsymbol{r}_{aq}\| = \|\boldsymbol{a}_a - \boldsymbol{q}_q\|$.

Being $G_{aq}(r_{aq}, \omega)$ and ΔS_q function of the locations of the N_a discrete points in the acoustic domain and of the N_q points on the structure, they can be grouped in a *complex-valued collocation matrix* $\boldsymbol{T}_{\boldsymbol{a}\boldsymbol{q}}(\omega)$, sized $N_a \times N_q$, of element $T_{aq}(\omega) = -2\omega^2\rho_0 G_{aq}(r_{aq}, \omega)\Delta S_q$, to transform Eq.2 into:

$$p(\boldsymbol{a}_a, \omega) \approx \boldsymbol{T}_{\boldsymbol{a}\boldsymbol{q}}(\omega)\boldsymbol{H}_{\boldsymbol{d}_n\boldsymbol{q}f}(\omega)\boldsymbol{F}_f(\omega) \in \mathbb{C}. \tag{3}$$

If, similarly to the *acoustic transfer vectors* in Gérard et al. (2002); Citarella et al. (2007), an *acoustic transfer matrix* $\boldsymbol{V}_{\boldsymbol{a}\boldsymbol{f}}(\omega)$, sized $N_a \times N_f$, is defined as:

$$\boldsymbol{V}_{\boldsymbol{a}\boldsymbol{f}}(\omega) = \boldsymbol{T}_{\boldsymbol{a}\boldsymbol{q}}(\omega) \cdot \boldsymbol{H}_{\boldsymbol{d}_n\boldsymbol{q}\boldsymbol{f}}(\omega) \in \mathbb{C}, \tag{4}$$

Eq.3 can be easily rewritten as:

$$p(\boldsymbol{a}_a, \omega) \approx \boldsymbol{V}_{af}(\omega)\boldsymbol{F}_f(\omega) \in \mathbb{C}, \tag{5}$$

useful in the cases where the structural response and acoustic domains are kept unchanged, while varying only the excitation signature to map the responses on the acoustic pressure field.

2.1. Notes: indirect excitation force retrieval from sound pressure fields

By reversing Eq.5, with the use of the *pseudo-inverse* of the *acoustic transfer matrix* $\boldsymbol{V}_{\boldsymbol{a}\boldsymbol{f}}(\omega)$ of Eq.4, the forces induced on the structure at the excitation/shaker head by a known *complex-valued* pressure field can be retrieved:

$$\hat{\boldsymbol{F}}_f(\omega) \approx \boldsymbol{V}^+_{\boldsymbol{f}\boldsymbol{a}}(\omega)\boldsymbol{p}(\boldsymbol{a}, \omega) \in \mathbb{C}. \tag{6}$$

with the *pseudo-inverse* of the *acoustic transfer matrix* $\boldsymbol{V}_{\boldsymbol{a}\boldsymbol{f}}(\omega)$, sized $N_f \times N_a$ and callable $\boldsymbol{V}^+_{\boldsymbol{f}\boldsymbol{a}}(\omega)$, precisely as:

$$\boldsymbol{V}^+_{\boldsymbol{f}\boldsymbol{a}}(\omega) = [\boldsymbol{V}^H_{\boldsymbol{f}\boldsymbol{a}}(\omega)\boldsymbol{V}_{\boldsymbol{a}\boldsymbol{f}}(\omega)]^{-1}\boldsymbol{V}^H_{\boldsymbol{f}\boldsymbol{a}}(\omega) \in \mathbb{C}. \tag{7}$$

The matrix $\boldsymbol{V}^H_{\boldsymbol{f}\boldsymbol{a}}(\omega)\boldsymbol{V}_{\boldsymbol{a}\boldsymbol{f}}(\omega)$, to be inverted at each angular frequency ω, is a *complex-valued* square matrix of size $N_f \times N_f$, but this time N_f is very small or unity, simplifying the inversion.

3. Full Field FRFs: direct experimental modelling

3.1. Brief recall of a direct characterisation

The formulation of *receptance* matrix $\boldsymbol{H_d}(\omega)$, taken from Ewins (2000); Heylen et al. (1998) as spectral relation between displacements and forces, will be used for the *full-field FRF estimation*, describing the dynamic behaviour of a testing system, with potentially multi-input excitation, here 2 distinct shakers, and *many*-output responses, here also several thousands, covering the whole sensed surface, as can be formulated in the following *complex-valued* equation:

$$H_{d_{qf}}(\omega) = \frac{\sum_{m=1}^{N} S^{m}_{X_q F_f}(\omega)}{\sum_{m=1}^{N} S^{m}_{F_f F_f}(\omega)} \in \mathbb{C} \tag{8}$$

where X_q is the output displacement at q-th dof induced by the input force F_f at f-th dof, while $S^{m}_{X_q F_f}(\omega)$ is the m-th cross power spectral density between input and output, $S^{m}_{F_f F_f}(\omega)$ is the m-th auto power spectral density of the input and ω is the angular frequency, evaluated in N repetitions.

3.2. Brief summary of the technological equipment

To the interested reader, the most detailed notes on the test campaign appeared in Zanarini (2019a), with further suggestions in Zanarini (2019b, 2020, 2022b), but here is a brief summary of what was available at TU-Wien as in Fig.1: a dedicated seismic floor room; a mechanical & electronic workshop with technicians; traditional tools for vibration & modal analysis; but, in particular, there were SLDV, Hi-Speed DIC and ESPI measurement instruments.

Accurate studies were needed to understand each technological limit and if a common test for concurrent usage might have been really possible. All this brought to a unique set-up for the comparison of the 3 optical technologies in *full-field FRF estimations*; great attention was paid on the design of experiments for further research in modal analysis. After an accurate tuning, a feasible performance overlapping was sought directly out of each instrument, reminding that the same structural dynamics can be sensed in complementary domains, which means frequency for SLDV & ESPI, time for DIC. Topology transforms were added to have the datasets in the same physical references.

4. Numerical mapping of sound pressure from full-field *receptances* & first steps of inverse vibro-acoustics

The relevance of the defined *acoustic transfer matrix* $\boldsymbol{V_{af}}(\omega)$ should be clear, also in sight of its *pseudo-inverse* $\boldsymbol{V^{+}_{fa}}(\omega)$ evaluation in Eq.7, before the adoption of a specific excitation signature, to simulate the acoustic pressure in Eq.5 and the identified force in Eq.6. Examples with the *full-field receptances* are here given.

4.1. Meshing the acoustic domain

For the aims of this paper, a squared mesh was generated, of size $0.5m \times 0.5m$, with 51×51 dofs ($N_a = 2601$, $10mm$ as acoustic grid spacing), centred on the vibrating plate and positioned $0.1m$ above it. The air parameters were fixed in $c_0 = 300.0m/s$ and $\rho_0 = 1.204kg/m^3$.

4.2. Evaluation of the acoustic transfer matrix

The core of this paper is to show the possibility to evaluate the *acoustic transfer matrix* $\boldsymbol{V_{aq}}(\omega)$ directly from the *experiment-based receptances*, as proposed in Section 2, without the need of any FE structural model, but with great detail and field quality. It is important to underline how the *acoustic transfer matrix* obtained from the *experiment-based receptances* preserves, with its *complex-valued nature*, the real life conditions of the test, without any simplification in the damping, nor in the materials' properties, nor in the boundary conditions, nor in the modal base truncation

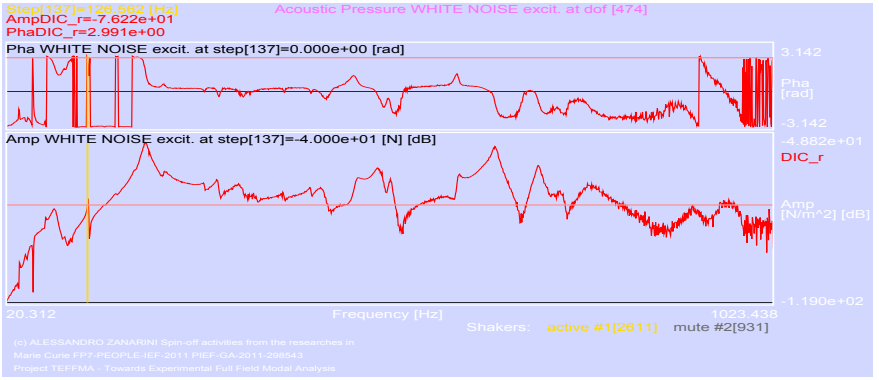

Fig. 2. Example of *acoustic pressure* graph in the frequency domain evaluated in acoustic dof 474 with *white noise* excitation from shaker 1.

or identification. In Fig.2 an example of the *acoustic transfer matrix* $\boldsymbol{V_{aq}}(\omega)$ is reported as a frequency domain relation from shaker 1 and acoustic dof 474 here selected in the squared acoustic mesh.

In the proofs organised in Fig.3, the *white noise* amplitude spectrum $F(\omega)$ was used in the shape of $F(\omega) = F_0/\omega^{\alpha}$, $\alpha = 0$, $F_0 = 0.01N$, with excitation from shaker 1, therefore just scaling the *acoustic transfer matrix*. The results of the latter are shown over the entire acoustic mesh, retaining again the *complex-valued* relations and phase delays, coming from the underneath *complex-valued receptance* matrix $\boldsymbol{H_{d_n qf}}(\omega)$, but blended in the *complex-valued* summation in $\boldsymbol{V_{aq}}(\omega)$. It appears also manifest how the distance on the acoustic mesh plays a relevant role in blending, or averaging, the contributions of specific areas on the vibrating plate, revealing in particular the proximity to specific nodal lines of the structural ODSs. In Fig.3*a* the acoustic pressure field is shown to exhibit a clear link to the *receptance* shape (in front), as the latter is quite simple at 127 Hz. As the frequency rises, more shape complexity pertains the *receptance* maps, as can be clearly seen in Fig.3*b* at 820 Hz, but the resulting complex-valued blending in the acoustic pressure field, taking account of all the contributions across the radiating surface, properly phased, now has a different shape, coming from the complex-valued summation of $N_q = 2907$ contributing Green's functions in Eq.2.

4.3. Evaluation of the inverse airborne vibro-acoustic FRFs

Following the formulation of Eq.7, the *pseudo-inverse vibro-acoustic FRFs* $\boldsymbol{V^{+}_{fa}}(\omega)$ (or *pseudo-inverse acoustic transfer matrix*) of force over airborne sound pressure can be achieved, as shown in the single inverse vibro-acoustic FRF of Fig.4, where the airborne pressure field is considered acting on the single acoustic dof 474 and the force in the structural dof 2611 of the shaker 1. It can be clearly appreciated how the whole complex-valued information is retained in the pseudo-inversion, up to the numerical precision of the routines.

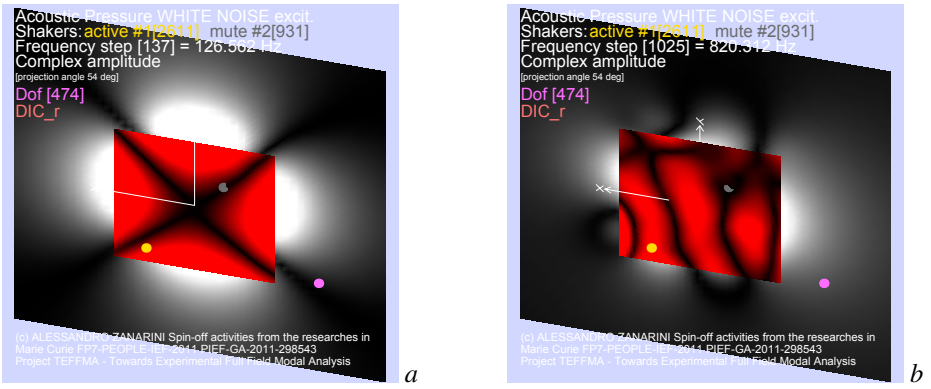

Fig. 3. Examples of *acoustic pressure* mesh evaluated at the specific frequencies of 127 & 820 Hz, *white noise* excitation from shaker 1.

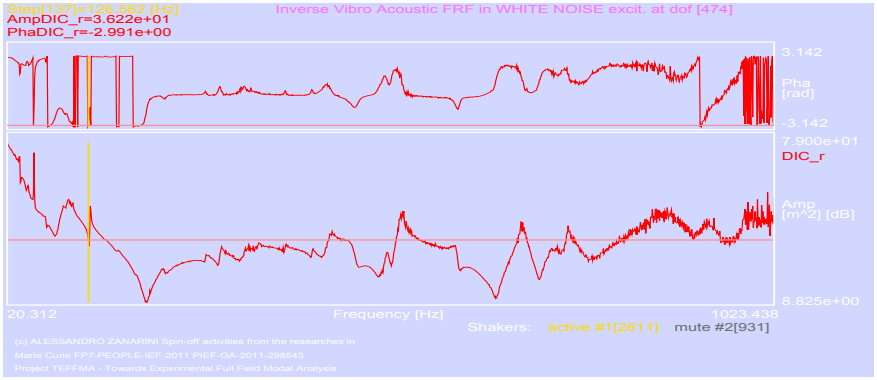

Fig. 4. Example of *inverse vibro-acoustic FRF* graph in the frequency domain evaluated as force in shaker 1 over the airborne acoustic pressure from dof 474.

4.4. Identification of the force induced by the airborne acoustic field

For the identification of the force $\hat{F}_1(\omega)$ in the structural dof 2611 of the shaker 1, by means of Eq.6, the whole airborne pressure field acting on all the dofs of the acoustic mesh must be used, together with all the *pseudo-inverse vibro-acoustic FRFs* in Section 4.3. The *white noise* excitation on shaker 1 was adopted to simulate the pressure field without any scaling and phasing biases in the whole frequency range of interest. Furthermore, the acoustic pressure coming from the *white noise* excitation permits to boldly highlight how the difference between the original excitation and the identified force is in the range of machine precision of `double` floating precision, or machine epsilon of $2^{-52} \approx 2.22e{-}16$. In Fig.5 the original *white noise* excitation $F(\omega) = F_0$ (in black), with even amplitude and no phase lag on the whole frequency domain, and the identified force $\hat{F}_1(\omega)$ (in red) are show together. To be noted how the amplitude extremes are labelled in the same manner, as truncated only at the 3rd decimal, while 16+1 decimals would be needed to show properly the difference in its range $[1.402e{-}16, 2.207e{-}16]$; instead the amplitude graphs are magnified to appreciate the differences in the narrow range of the errors, while phase is completely superimposed.

5. Conclusions

This paper has highlighted the chance to retrieve structural excitation informations from airborne acoustic fields, opening inquiry's possibilities in NVH and coupled fluid-structural dynamics, coming from *experiment-based optical full-field tools* for an advancement of experimental benchmarks of design procedures of complex structures. The unprecedented mapping ability, in both spatial and frequency domains, opens new cross vibro-acoustic prediction

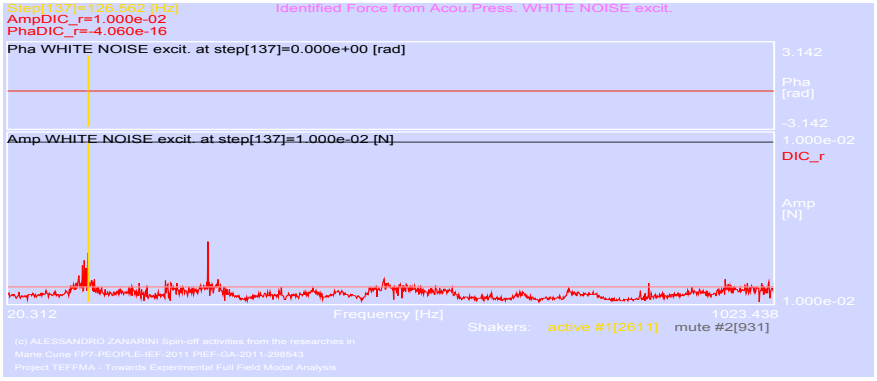

Fig. 5. Example of *identified force* graph in the frequency domain evaluated as force in shaker 1 from the whole airborne acoustic pressure field.

scenarios, as the real-life structural dynamics of the radiating surface is entirely retained in the *receptances* with great accuracy, but without assumptions nor errors in any modal identification nor in any virtual modelling.

Acknowledgements

The European Commission Research Executive Agency is acknowledged for funding the project TEFFMA - Towards Experimental Full Field Modal Analysis, funded by the European Commission at the Technische Universitaet Wien, Austria, through the Marie Curie FP7-PEOPLE-IEF-2011 PIEF-GA-2011-298543 grant in years 2013-2015.

References

Citarella, R., Federico, L., Cicatiello, A., 2007. Modal acoustic transfer vector approach in a fem–bem vibro-acoustic analysis. Engineering Analysis with Boundary Elements 31, 248–258. doi:10.1016/j.enganabound.2006.09.004.

Desmet, W., 2004. Boundary element method in acoustics. Technical Report. Katholieke Universiteit Leuven, Belgium, Mechanical Engineering Department, Noise & Vibration research group, URL: https://www.mech.kuleuven.be/en/research/. In ISAAC 15 - Course on numerical and applied acoustics, Katholieke Universiteit Leuven, Belgium, Mechanical Engineering Department, Noise & Vibration research group, URL: https://www.isma-isaac.be.

Ewins, D.J., 2000. Modal Testing - theory, practice and application. 2nd ed., Research Studies Press Ltd., Baldock, Hertfordshire, England. URL: https://www.wiley.com/en-it/Modal+Testing%3A+Theory%2C+Practice+and+Application%2C+2nd+Edition-p-9780863802188.

Gérard, F., Tournour, M., Masri, N., Cremers, L., Felice, M., Selmane, A., 2002. Acoustic transfer vectors for numerical modeling of engine noise. Sound and Vibration 36, 20–25.

Heylen, W., Lammens, S., Sas, P., 1998. Modal Analysis Theory and Testing. 2nd ed. ed., Katholieke Universiteit Leuven, Leuven (Belgium). ISBN 90-73802-61-X.

Kirkup, S., 1994. Computational solution of the acoustic field surrounding a baffled panel by the rayleigh integral method. Applied Mathematical Modelling 18, 403–407. doi:10.1016/0307-904X(94)90227-5.

Kirkup, S., 2019. The boundary element method in acoustics: A survey. Applied Sciences 9. doi:10.3390/app9081642.

Kirkup, S., Thompson, A., 2007. Computing the acoustic field of a radiating cavity by the boundary element - rayleigh integral method (BERIM), in: Ao, S.I., Gelman, L., Hukins, D.W.L., Hunter, A., Korsunsky, A.M. (Eds.), World Congress on Engineering, WCE 2007, London, UK, July 2-4 , 2007, Newswood Limited. pp. 1401–1406. URL: http://www.kirkup.info/papers/SKAT07.pdf.

Mas, P., Sas, P., 2004. Acoustic source identification based on microphone array processing. Technical Report. Katholieke Universiteit Leuven, Belgium, Mechanical Engineering Department, Noise & Vibration research group, URL: https://www.mech.kuleuven.be/en/research/. In ISAAC 15 - Course on numerical and applied acoustics, Katholieke Universiteit Leuven, Belgium, Mechanical Engineering Department, Noise & Vibration research group, URL: https://www.isma-isaac.be.

Van der Auweraer, H., Steinbichler, H., Haberstok, C., Freymann, R., Storer, D., Linet, V., 2001. Industrial applications of pulsed-laser espi vibration analysis, in: Proc. of the XIX IMAC, Kissimmee, FL, USA, SEM. pp. 490–496. URL: https://www.researchgate.net/publication/238246330_Industrial_Applications_of_Pulsed-Laser_ESPI_Vibration_Analysis.

Wind, J., Wijnant, Y., de Boer, A., 2006. Fast evaluation of the Rayleigh integral and applications to inverse acoustics, in: Proceedings of the ICSV13, The Thirteenth International Congress on Sound and Vibration, Vienna, Austria, July 2-6, 2006, International Institute of Acoustics and Vibration (IIAV). pp. 1–8.

Zanarini, A., 2005a. Damage location assessment in a composite panel by means of electronic speckle pattern interferometry measurements, in: Proceedings of the IDETC/CIE ASME International Design Engineering Technical Conferences & Computers and Information in Engineering Conference, Long Beach, California, USA, September 24-28, ASME. pp. 1–8. doi:10.1115/DETC2005-84631. paper DETC2005-84631.

Zanarini, A., 2005b. Dynamic behaviour carachterization of a brake disc by means of electronic speckle pattern interferometry measurements, in: Proceedings of the IDETC/CIE ASME International Design Engineering Technical Conferences & Computers and Information in Engineering Conference, Long Beach, California, USA, September 24-28, ASME. pp. 273–280. doi:10.1115/DETC2005-84630. paper DETC2005-84630.

Zanarini, A., 2007. Full field ESPI measurements on a plate: challenging experimental modal analysis, in: Proceedings of the XXV IMAC, Orlando (FL) USA, Feb 19-22, SEM. pp. 1–11. URL: https://www.researchgate.net/publication/266896551_Full_field_ESPI_measurements_on_a_plate_Challenging_Experimental_Modal_Analysis. paper s34p04.

Zanarini, A., 2008a. Fatigue life assessment by means of full field ESPI vibration measurements, in: Sas, P. (Ed.), Proceedings of the ISMA2008 Conference, September 15-17, Leuven (Belgium), KUL. pp. 817–832. doi:10.13140/RG.2.1.3452.9365. Condition monitoring, Paper 326.

Zanarini, A., 2008b. Full field ESPI vibration measurements to predict fatigue behaviour, in: Proceedings of the IMECE2008 ASME International Mechanical Engineering Congress and Exposition, October 31- November 6, Boston (MA) USA, ASME. pp. 165–174. doi:10.1115/IMECE2008-68727. paper IMECE2008-68727.

Zanarini, A., 2014a. On the estimation of frequency response functions, dynamic rotational degrees of freedom and strain maps from different full field optical techniques, in: Proceedings of the ISMA2014 including USD2014 - International Conference on Noise and Vibration Engineering, Leuven, Belgium, September 15-17, KU Leuven. pp. 1177–1192. URL: http://past.isma-isaac.be/downloads/isma2014/papers/isma2014_0676.pdf. Dynamic testing: methods and instrumentation, paper ID676.

Zanarini, A., 2014b. On the role of spatial resolution in advanced vibration measurements for operational modal analysis and model updating, in: Proceedings of the ISMA2014 including USD2014 - International Conference on Noise and Vibration Engineering, Leuven, Belgium,

September 15-17, KU Leuven. pp. 3397–3410. URL: http://past.isma-isaac.be/downloads/isma2014/papers/isma2014_0678.pdf. Operational modal analysis, paper ID678.

Zanarini, A., 2015a. Accurate FRFs estimation of derivative quantities from different full field measuring technologies, in: Proceedings of the ICoEV2015 International Conference on Engineering Vibration, Ljubljana, Slovenia, September 7-10, Univ. Ljubljana & IFToMM. pp. 1569–1578. URL: https://www.researchgate.net/publication/280013778_Accurate_FRF_estimation_of_derivative_quantities_from_different_full_field_measuring_technologies. ID192.

Zanarini, A., 2015b. Comparative studies on full field FRFs estimation from competing optical instruments, in: Proceedings of the ICoEV2015 International Conference on Engineering Vibration, Ljubljana, Slovenia, September 7-10, Univ. Ljubljana & IFToMM. pp. 1559–1568. URL: https://www.researchgate.net/publication/280013709_Comparative_studies_on_Full_Field_FRFs_estimation_from_competing_optical_instruments. ID191.

Zanarini, A., 2015c. Full field experimental modelling in spectral approaches to fatigue predictions, in: Proceedings of the ICoEV2015 International Conference on Engineering Vibration, Ljubljana, Slovenia, September 7-10, Univ. Ljubljana & IFToMM. pp. 1579–1588. URL: https://www.researchgate.net/publication/280013788_Full_field_experimental_modelling_in_spectral_approaches_to_fatigue_predictions. ID193.

Zanarini, A., 2015d. Model updating from full field optical experimental datasets, in: Proceedings of the ICoEV2015 International Conference on Engineering Vibration, Ljubljana, Slovenia, September 7-10, Univ. Ljubljana & IFToMM. pp. 773–782. URL: https://www.researchgate.net/publication/280013876_Model_updating_from_full_field_optical_experimental_datasets. ID196.

Zanarini, A., 2018. Broad frequency band full field measurements for advanced applications: Point-wise comparisons between optical technologies. Mechanical Systems and Signal Processing 98, 968 – 999. doi:10.1016/j.ymssp.2017.05.035.

Zanarini, A., 2019a. Competing optical instruments for the estimation of Full Field FRFs. Measurement 140, 100 – 119. doi:10.1016/j.measurement.2018.12.017.

Zanarini, A., 2019b. Full field optical measurements in experimental modal analysis and model updating. Journal of Sound and Vibration 442, 817 – 842. doi:10.1016/j.jsv.2018.09.048.

Zanarini, A., 2020. On the making of precise comparisons with optical full field technologies in NVH, in: ISMA2020 including USD2020 - International Conference on Noise and Vibration Engineering, Leuven, Belgium, September 7-9, KU Leuven. pp. 2293–2308. URL: https://past.isma-isaac.be/downloads/isma2020/proceedings/Contribution_695_proceeding_3.pdf. Optical methods and computer vision for vibration engineering, paper ID 695.

Zanarini, A., 2022a. About the excitation dependency of risk tolerance mapping in dynamically loaded structures, in: ISMA2022 including USD2022 - International Conference on Noise and Vibration Engineering, Leuven, Belgium, September 12-14, KU Leuven. pp. 3804–3818. URL: https://past.isma-isaac.be/downloads/isma2022/proceedings/Contribution_208_proceeding_3.pdf. paper ID 208 in Vol. Structural Health Monitoring.

Zanarini, A., 2022b. Chasing the high-resolution mapping of rotational and strain FRFs as receptance processing from different full-field optical measuring technologies. Mechanical Systems and Signal Processing 166, 108428. doi:10.1016/j.ymssp.2021.108428.

Zanarini, A., 2022c. Introducing the concept of defect tolerance by fatigue spectral methods based on full-field frequency response function testing and dynamic excitation signature. International Journal of Fatigue 165, 107184. doi:10.1016/j.ijfatigue.2022.107184.

Zanarini, A., 2022d. On the approximation of sound radiation by means of experiment-based optical full-field receptances, in: ISMA2022 including USD2022 - International Conference on Noise and Vibration Engineering, Leuven, Belgium, September 12-14, KU Leuven. pp. 2735–2749. URL: https://past.isma-isaac.be/downloads/isma2022/proceedings/Contribution_207_proceeding_3.pdf. paper ID 207 in Vol. Optical Methods.

Zanarini, A., 2022e. On the defect tolerance by fatigue spectral methods based on full-field dynamic testing. Procedia Structural Integrity 37, 525–532. doi:10.1016/j.prostr.2022.01.118. paper ID 105, ICSI 2021 The 4th International Conference on Structural Integrity.

Zanarini, A., 2022f. On the exploitation of multiple 3D full-field pulsed ESPI measurements in damage location assessment. Procedia Structural Integrity 37, 517–524. doi:10.1016/j.prostr.2022.01.117. paper ID 104, ICSI 2021 The 4th International Conference on Structural Integrity.

Zanarini, A., 2023a. Experiment-based optical full-field receptances in the approximation of sound radiation from a vibrating plate, in: IMAC XLI - International Modal Analysis Conference - Keeping IMAC Weird: Traditional and Non-traditional Applications of Structural Dynamics, Austin (Texas), USA, Springer Nature Switzerland AG & SEM Society for Experimental Mechanics. pp. 1–13. doi:10.1007/978-3-031-34910-2_4. paper ID 14650 - chapter 4, in J. Baqersad, D. Di Maio (eds.), Computer Vision & Laser Vibrometry, Volume 6, Conference Proceedings of the Society for Experimental Mechanics Series.

Zanarini, A., 2023b. On the influence of scattered errors over full-field receptances in the Rayleigh integral approximation of sound radiation from a vibrating plate. Acoustics 5, 948–986. URL: https://www.mdpi.com/2624-599X/5/4/55, doi:10.3390/acoustics5040055.

Zanarini, A., 2023c. Risk tolerance mapping in dynamically loaded structures as excitation dependency by means of full-field receptances, in: IMAC XLI - International Modal Analysis Conference - Keeping IMAC Weird: Traditional and Non-traditional Applications of Structural Dynamics, Austin (Texas), USA, Springer Nature Switzerland AG & SEM Society for Experimental Mechanics. pp. 43–56. doi:10.1007/978-3-031-34910-2_9. paper ID 14648 - chapter 9, in J. Baqersad, D. Di Maio (eds.), Computer Vision & Laser Vibrometry, Volume 6, Conference Proceedings of the Society for Experimental Mechanics Series.